




Investigation of a Radio-Iodinated Alpha-Mangostin for Targeting Estrogen Receptor Alpha (ER α) in Breast Cancer: In Silico Design, Synthesis, and Biological Evaluation

Muchtaridi Muchtaridi ^{1,2}, Wiwit Nurhidayah¹, Taufik Muhammad Fakhri ^{1,3}, Kento Kannaka⁴, Hiroyuki Suzuki ⁴, Toto Subroto⁵, Tomoya Uehara⁴

¹Department of Pharmaceutical Analysis and Medicinal Chemistry, Faculty of Pharmacy, Universitas Padjadjaran, Sumedang, 45363, Indonesia;

²Research Collaboration Centre for Radiopharmaceuticals Theranostic, National Research and Innovation Agency (BRIN), Sumedang, 45363, Indonesia; ³Department of Pharmacy, Faculty of Mathematics and Natural Sciences, Universitas Islam Bandung, Bandung, 40116, Indonesia; ⁴Graduate School of Pharmaceutical Sciences, Chiba University, Chiba, 260-8675, Japan; ⁵Department of Chemistry, Faculty of Mathematics and Natural Sciences, Universitas Padjadjaran, Sumedang, 45363, Indonesia

Correspondence: Tomoya Uehara; Muchtaridi Muchtaridi, Email tuehara@chiba-u.jp; muchtaridi@unpad.ac.id

Introduction: Alpha-mangostin (AM), the most representative xanthone derivative isolated from the rind of the Purple Mangosteen (*Garcinia mangostana* Linn), has been reported pharmacologically to be associated with breast cancer in silico, in vitro, and in vivo. Although the pharmacological effects of AM are believed to involve the estrogen receptor alpha (ER α), there are no reports available in the literature describing the binding of AM to ER α .

Methods: In this study, iodine-125 (¹²⁵I)-labeled AM ([¹²⁵I]I-AM) was prepared, and its binding to ER α was investigated in vitro using MCF-7 cell lines. To investigate the applicability of radioiodine-labeled AM as a radiopharmaceutical for breast cancer, [¹²⁵I]I-AM was injected into nude mice bearing MCF-7.

Results: The results obtained showed that the uptake of [¹²⁵I]I-AM into MCF-7 cells was found to be inhibited by AM and tamoxifen, suggesting that its uptake is partially mediated by ER α . In addition, the biodistribution studies using MCF-7 bearing nude mice showed that [¹²⁵I]I-AM accumulated in tumor tissues, although deiodination did occur, reducing the concentration of iodine-125 (¹²⁵I) in the targeted cells.

Conclusion: These results suggested that AM would be a useful platform for the development of a new radiopharmaceutical targeting ER α . Further studies are, however, required to reduce deiodination of [¹²⁵I]I-AM in vivo.

Keywords: alpha-mangostin (AM), estrogen receptor alpha (ER α), breast cancer, radiopharmaceutical, iodine-125 (125I)

Introduction

Breast cancer is the most prevalent type of cancer in women. GLOBOCAN (*Global Cancer Observatory*) statistics indicate that 2.50 million new breast cancer cases (or 11.6% of all new cancer cases worldwide) were diagnosed in 2022.¹ Each year, an estimated 685,000 women lose their lives due to breast cancer, as reported by GLOBOCAN statistics.^{2,3} It is estimated that by 2040, the incidence of breast cancer will rise by over 3 million cases and 1 million mortality per year due to population expansion.⁴ More than 70% of breast cancers are classified as estrogen receptor-positive (ER+) breast cancers.⁵ There are two types of ERs: ER α and ER β . Through ER α , estrogen promotes cell growth while suppressing apoptosis, making ER α a prognostic indicator for breast cancer cases.^{6–8} Therefore, several anti-breast cancer drugs have been developed targeting ER α .⁷

Alpha-mangostin (AM, [Figure 1a](#)) is the most important xanthone derivative isolated from the rind of the Purple Mangosteen (*Garcinia mangostana* Linn) and has been shown to be active pharmacologically against breast cancer cells both through in vitro and in vivo studies.^{9–12} Through in silico studies, AM was found to demonstrate antagonistic

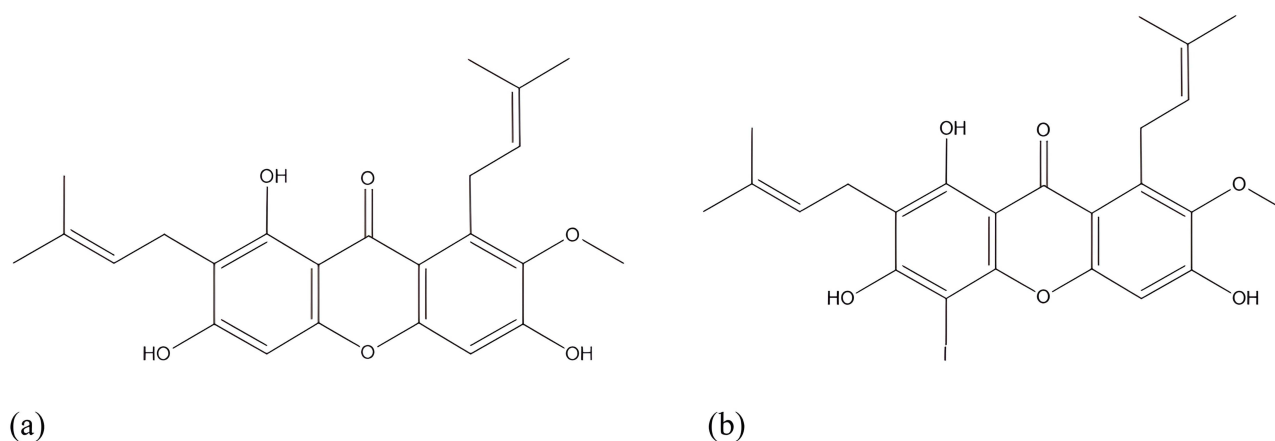


Figure 1 The structures of (a) AM and (b) I-AM.

activity against ER α , with a binding energy of -9.05 kcal/mol and a pharmacophore-fit score of 83.06% to 4-OHT.^{13–15} AM is also known to inhibit the growth of MCF-7 breast cancer cells by down-regulation of ER α expression.¹⁶ It inhibits the cell proliferation of the ER α -positive MCF-7 cell line. Meanwhile, ER-negative MDA-MB-231 cells were less responsive. Treatment of MCF-7 cells with 10 μ M AM for 48 hours mainly reduced the expression of ER α and pS2 and the genes that are sensitive to estrogen.¹⁷ These studies suggested that AM would be involved in ER α , but whether AM binds to ER α directly or not remains unclear.

In this study, iodine-125-labeled AM ([¹²⁵I]I-AM, Figure 1b) was synthesized following a 100 ns molecular dynamic simulation to predict the iodine substitution to AM. Subsequently, [¹²⁵I]I-AM was synthesized with non-isotope iodine, thus its structure could be elucidated according to the *in silico* predictions. The binding of [¹²⁵I]I-AM to ER α was then evaluated *in vitro* using MCF-7 breast cancer cells, and *in vivo* study was conducted on nude mice bearing MCF-7 tumor to evaluate the applicability of radioiodine-labeled AM as a radiopharmaceutical against breast cancer cells.

Results and Discussions

Several studies suggested the interaction between AM and ER α ,¹⁷ but it is unclear the exact mode of interaction between them. Therefore, this was explored in this study. The reactivity of [¹²⁵I]I-AM was calculated using Density Functional Theory (DFT), its stability was predicted using molecular dynamics simulations, and its interaction with ER α was evaluated using MCF-7 breast cancer cells following successful synthesis and characterization.

Computational Methodology

Calculated Structure of [¹²⁵I]I-AM Complex

Each molecule was subjected to optimization to reach its most stable conformation at the lowest energy state. During this process, molecules or atoms with high energy levels form bonds and release energy, which further stabilizes the system. The formation of [¹²⁵I]I-AM happens following the collision between AM with the iodine ions which triggers a reaction. The collision that provides sufficient energy exceeding the activation threshold will result in the formation of the complex at a lower energy level than the free AM. The decrease in energy in the [¹²⁵I]I-AM complex compared to free AM, as shown in Table 1, indicates a more stable interaction between AM and iodine. This can be attributed to the atomic configuration and ionic radii of iodine. It is known that iodine has relatively large ionic radii, approximately 198 pm for the iodine-125 isotope.¹⁷ With these large ionic radii, iodine has the potential to form bonds with AM in a more stable configuration, possibly by adopting a “sitting-atop” position on the AM molecule. Therefore, the interaction between positively charged AM and iodine ions can occur spontaneously due to the tendency to form stronger and more stable bonds based on the configuration and chemical properties of both substances.

The computational analysis of the DFT global chemical reactivity descriptor plays a significant role within conceptual DFT, as these metrics provide insights into the relationship among a molecule’s structure, stability, and reactivity.¹⁷

Table 1 The Molecular Energies of the Optimized Configurations and Overall Chemical Reactivity Descriptors for Positively Charged AM-Iodine Complexes

Parameters	Alfa-Mangostin Compounds	
	AM	[¹²⁵ I]-AM
E(RB3LYP)	-1381.34414825 a.u.	-1392.11431710 a.u.
RMS Gradient Norm	0.00000232 a.u.	0.00000215 a.u.
Dipole Moment	3.2595 Debye	2.1237 Debye
LUMO	-0.07587 hartree	-0.08025 hartree
HOMO	-0.21735 hartree	-0.21776 hartree
LUMO-HOMO Gap	0.14148 hartree	0.13751 hartree
Chemical Hardness (η)	0.07074 hartree	0.06876 hartree
Electronic Chemical Potential (μ)	-0.14661 hartree	-0.14901 hartree
Electrophilicity (ω)	2.07252 hartree	2.16710 hartree

These descriptors are derived from the evaluation of energy levels associated with the HOMO (Highest Occupied Molecular Orbital) and LUMO (Lowest Unoccupied Molecular Orbital) of the optimized molecule.¹⁷

The HOMO and LUMO contour plots of the [¹²⁵I]-AM complex provide an overview of how electrons are distributed between AM and iodine in the complex molecule (Figure 2). This electron distribution is associated with the d-orbital of iodine and the p-orbital of AM, where charge transfer occurs from iodine to AM. The dominance of the electron distribution around the core of the AM molecule indicates focused interactions in this region, reflecting the formation of stable bonds between the two components. As a result, the [¹²⁵I]-AM complex exhibits a well-organized structure, demonstrating significant charge transfer processes.

Chemical hardness (η) characterizes a molecule's resistance against changes or electron alterations, and it is closely correlated with the stability and reactivity of a chemical system.¹⁷ This parameter, represented by Equation (1), quantifies the energy gap that exists between the two frontier orbitals, namely the HOMO and LUMO. A molecule with high hardness exhibits a significant HOMO–LUMO gap, indicating enhanced stability and a higher requirement of excitation energy to achieve the excited states. As indicated in Table 1, [¹²⁵I]-AM demonstrates a high level of chemical hardness, suggesting reduced reactivity compared to its base form, AM.

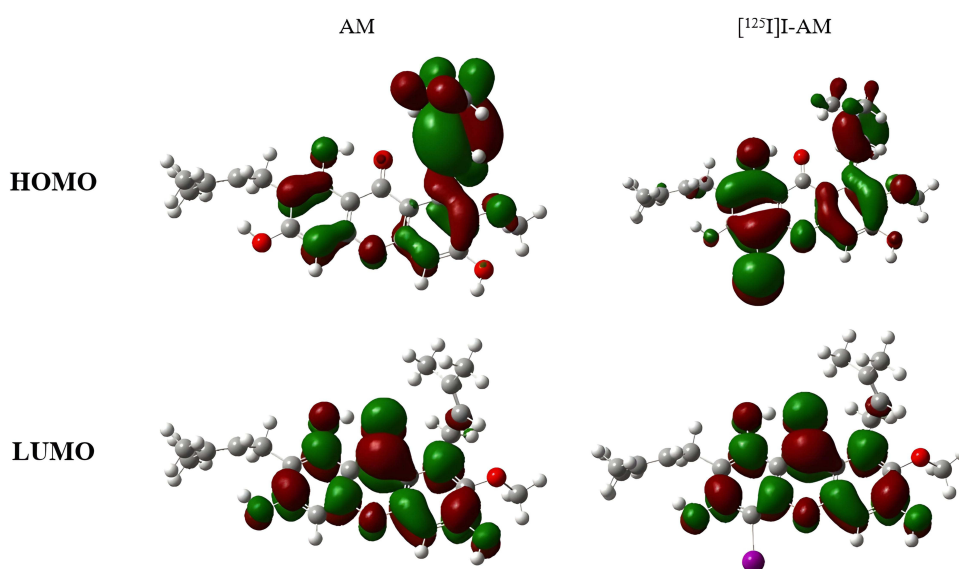


Figure 2 Electron distribution of AM (left) and [¹²⁵I]-AM (right) complexes, showcasing their intriguing properties.

The electronic chemical potential (μ) gauges the inclination of electrons to depart from an equilibrium system, akin to the electronegativity of the molecule.¹⁷ According to calculations employing Equation (2), [¹²⁵I]I-AM exhibits a diminished electronic chemical potential compared to its base form. This indicates heightened stability of the molecule, as it tends to retain electrons within the system, mitigating their escape.

Electrophilicity (ω) characterizes the ability of a species to accept electrons and measures the energy change when an electrophile interacts with a nucleophile.¹⁷ This parameter is determined through the amalgamation of chemical hardness and electronic chemical potential (Equation (3)). The analysis of electrophilicity indicates that [¹²⁵I]I-AM exhibits enhanced stability and reduced reactivity in terms of electron acceptance.

According to the global chemical reactivity descriptor of DFT, this finding indicates that the formation of the [¹²⁵I]I-AM complex results in greater stability compared to its base form. Conversely, the interaction between AM and iodine tends to form a more stable complex, as indicated by the calculation of the global chemical reactivity descriptor of DFT. Based on these findings, the [¹²⁵I]I-AM complex was evaluated through molecular dynamic simulation against the ER α macromolecule, allowing for a deeper analysis of the molecular interaction properties within the complex. Subsequently, this complex was synthesized to enable further experimental research on the [¹²⁵I]I-AM complex.

Molecular Docking Studies [¹²⁵I]I-AM Against ER α

Molecular docking is conducted under ideal and unchanging conditions, which may not always reflect the dynamic state of the interacting molecules in their natural environment. As a result, the complete molecular mechanism of this compound remains partially understood. Molecular docking facilitates the precise alignment of the ligand onto the macromolecule and determines the affinity energy value.¹⁷ In this investigation, molecular docking was conducted on the ER α receptor using AM and [¹²⁵I]I-AM compounds as experimental agents to understand their binding interactions and potential therapeutic implications. Despite its limitations in capturing dynamic molecular interactions, molecular docking provides valuable insights into the possible binding modes and strengths between the compounds and the receptor.

Molecular docking experiments were conducted on AM with the box positioned at coordinates X: 30.282, Y: -1.913, and Z: 24.207, measuring 64 × 60 × 60 points in size with a spacing of 0.375 Å. According to the results of molecular docking, [¹²⁵I]I-AM exhibited the highest affinity energy among the compounds, with an affinity energy value of -9.09 kcal/mol. This value surpasses that of AM, which had an affinity energy value of -7.99 kcal/mol, as depicted in Table 2. The higher affinity of [¹²⁵I]I-AM suggests it may bind more effectively to the target site compared to AM. This improvement in binding affinity could lead to enhanced specificity and sensitivity in diagnostic applications. Moreover, the results underscore the potential of [¹²⁵I]I-AM as a more promising candidate for further in vivo studies and clinical evaluation.

Discovery Studio software was used for visualization of the docking conformations to investigate the intermolecular bonds formed between the macromolecules and the respective ligands. The visual representations are illustrated in Figure 3. Figure 3 indicates that these compounds can form hydrogen bond interactions with amino acid MET343, while their interactions with ASP351 and THR347 are confined solely to hydrophobic interactions. Both amino acids play crucial roles in regulating transcriptional activation of ER α . Such interactions may influence the conformation and stability of the ligand-receptor complex, as well as modulate cellular responses to estrogen hormonal signals.^{18,19} The ability of these compounds to engage MET343 via hydrogen bonding may enhance their binding affinity and selectivity of the estrogen receptor. Furthermore, the differential interaction profiles with ASP351 and THR347 highlight the importance of hydrophobic contacts in stabilizing the complex. Understanding these interaction patterns could provide insights into the design of more effective ER α modulators with improved therapeutic potential.

Table 2 The Outcomes of Molecular Docking Experiments Involving the Interaction of ER α with AM and [¹²⁵I]I-AM

AM Compounds	Affinity	Inhibition Constant
AM	-7.99 kcal/mol	1.39 μ M (micromolar)
[¹²⁵ I]I-AM	-9.09 kcal/mol	219.01 nM (nanomolar)

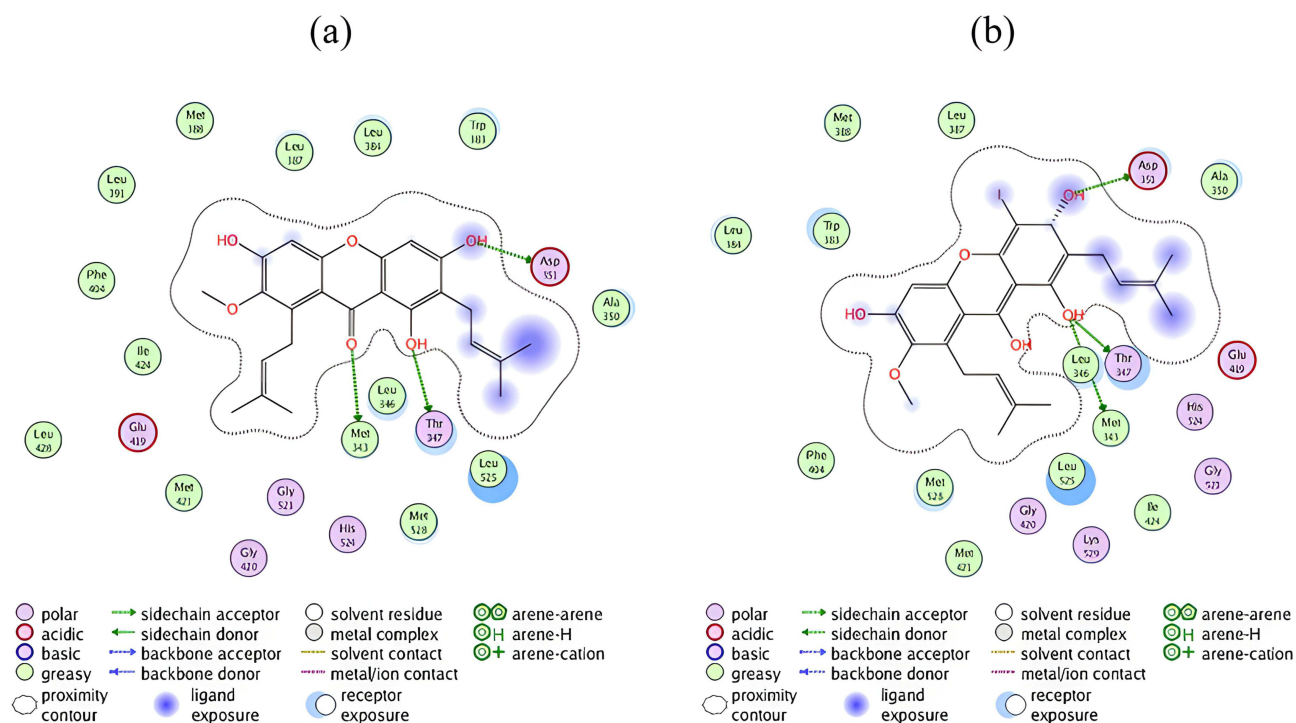


Figure 3 Depicts the intermolecular interaction between the compounds (a) AM and (b) [¹²⁵I]-AM with ER α .

Molecular Dynamics (MD) Simulations [¹²⁵I]-AM Against ER α

MD simulations were conducted for 100 ns to evaluate the stability of protein structures and the conformational alterations within the docked ligand complexes. Trajectory files generated from the MD simulations were scrutinized for various parameters, including root-mean-square deviation (RMSD), root mean square fluctuation (RMSF), radius of gyration (Rg), solvent-accessible surface area (SASA), secondary structure analysis, and hydrogen bond occupancy. These analyses helped in examining the stability and structural dynamics throughout the MD simulations.

RMSD serves to gauge the disparity between the starting and concluding positions of a protein. The smaller the RMSD, the more stable the configuration would be.¹⁷ For both ER α -AM and ER α -[¹²⁵I]-AM, their respective average RMSD values are 0.35 nm and 0.33 nm (Table 3). Remarkably, ER α -[¹²⁵I]-AM exhibits a lower RMSD value, which shows the complex is remarkably stable throughout the simulation, suggesting a robust binding to the ER α receptor with potential inhibitory activity. RMSF delineates residue-level fluctuations.¹⁷ Analysis of the ER α -[¹²⁵I]-AM complex RMSF plot reveals that residues MET343, ASP351, and THR347, interact with the ER α receptor's active site, manifesting a lower RMSF value compared to the ER α -AM complex (Figure 4b), which signifies stability upon binding.

The radius of gyration (Rg) indicates protein compactness.¹⁷ The mean Rg values for ER α -AM and ER α -[¹²⁵I]-AM are 1.90 nm and 1.88 nm, respectively (Table 3). This suggests that ER α -[¹²⁵I]-AM shows much higher binding affinity than ER α -AM. SASA represents the surface area of a protein that engages with the solvent molecules.¹⁷ The calculated average SASA values for ER α -AM and ER α -[¹²⁵I]-AM stand at 135.24 nm² and 130.21 nm², respectively. This suggests an augmentation in the ER α receptor's total SASA, implying that internal residues within the ER α receptor become solvent-accessible upon [¹²⁵I]-AM binding (Figure 4d).

Table 3 The Mean Values of RMSD, RMSF, Rg, and SASA for the ER α Receptor Throughout the 100 ns of Molecular Dynamics Simulations

Complex	RMSD (nm)	RMSF (nm)	Rg (nm)	SASA (nm ²)
ER α - AM	0.35	0.17	1.90	135.24
ER α - [¹²⁵ I]-AM	0.33	0.15	1.88	130.21

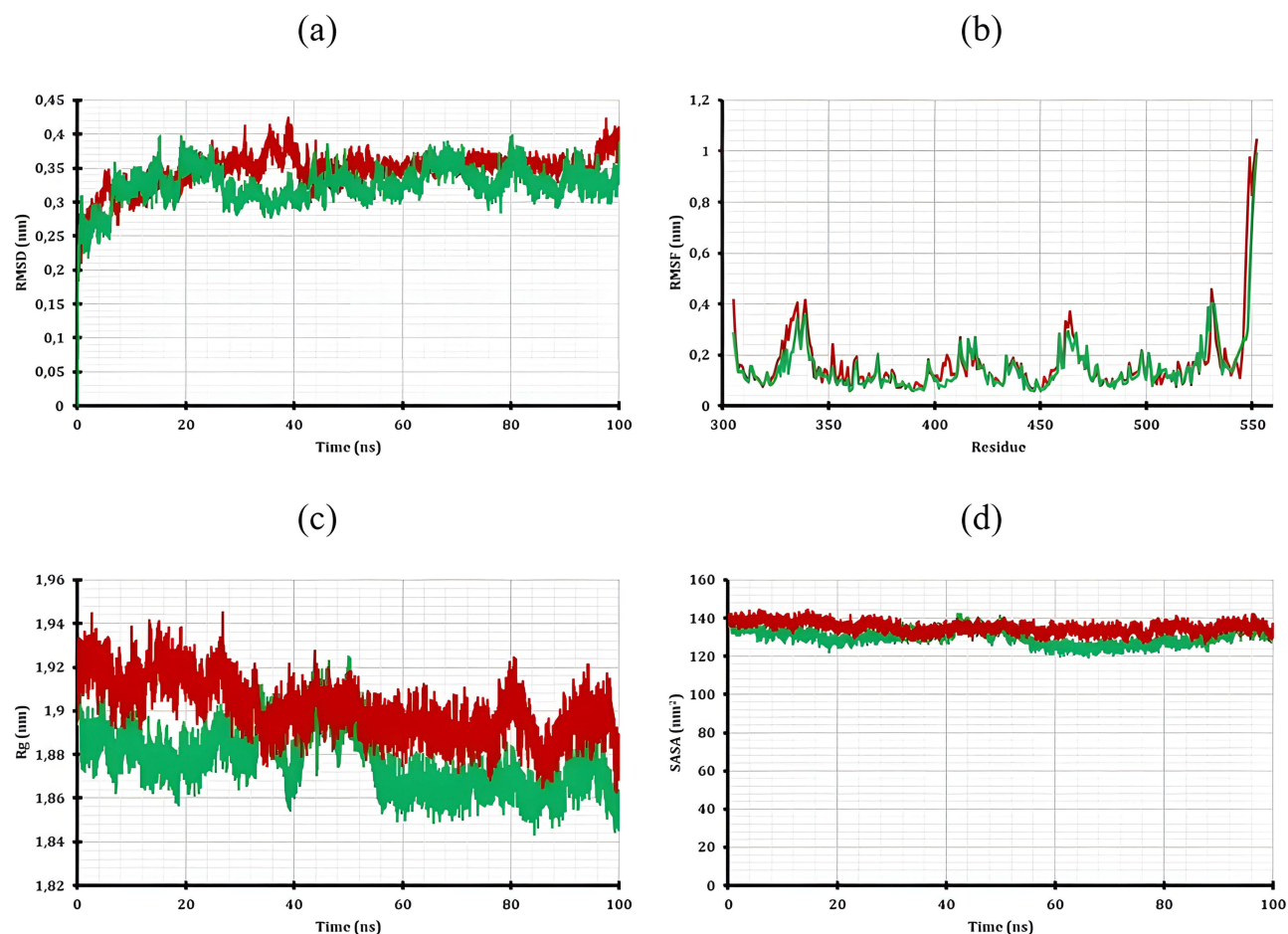


Figure 4 The ER α receptor's structural dynamics were analyzed using various parameters: (a) Root mean square deviation (RMSD), (b) Root mean square fluctuations (RMSF), (c) Radius of gyration (Rg), and (d) Solvent-accessible surface area (SASA). In the graphs, the ER α -AM form is represented in red, while the ER α -[125 I]I-AM form is depicted in green.

Hydrogen bonds play a crucial role in maintaining the stability of a ligand-protein complex.¹⁷ To confirm the structural stability, hydrogen bonds formed within a distance of 3.5 Å, as per the hydrogen bond criterion, were assessed in a solvent environment during the 100 ns MD simulations (Table 4). Notably, the occupancy of residues at the active site revealed that ASP351 was the primary contributor, with occupancies of 3.27% (AM) and 25.03% ([125 I]I-AM),

Table 4 The Interaction of Residues and the Occupancy Percentage of Hydrogen Bonds from the Simulation Trajectories

Complex	H-Bond Donor	H-Bond Acceptor	H-Bond Occupancy (%)	Total (%)
ER α - AM	AM	ASP351	3.27	6.89
	ASN532	AM	1.16	
	AM	ASN532	0.94	
	AM	MET388	0.01	
	AM	ASN532	1.41	
	HIS524	AM	0.08	
	AM	LEU384	0.01	
	ASN532	AM	0.01	
ER α - [125 I]I-AM	[125 I]I-AM	ASP351	25.03	36.37
	[125 I]I-AM	GLU353	9.58	
	THR347	[125 I]I-AM	0.01	
	ASN532	[125 I]I-AM	0.49	
	[125 I]I-AM	ASN532	1.26	

respectively. This underscores the importance of this residue in the structural integrity of the ER α receptor. The greatest number of hydrogen bonds (eight) was observed between AM and the ER α receptor, followed by the [125 I]I-AM compound, with five hydrogen bonds forming throughout the 100 ns MD simulations. However, the total hydrogen bond occupancy was highest in the ER α -[125 I]I-AM complex, at 36.37%. While the results of the hydrogen bond analysis align with the docking outcomes, the discrepancy in the number of hydrogen bonds between the two approaches could be attributed to the dynamics of ligand-protein interactions and conformational changes during MD simulation.

Binding Free Energy Calculations [125 I]I-AM Against ER α

The analysis above indicates that the ER α receptor undergoes conformational changes when binding to both AM and [125 I]I-AM compounds. However, this study is primarily focused on the binding affinity rankings of the two complex systems. Therefore, the binding free energies were calculated using the MM-PBSA approach based on 100 snapshots extracted from the stable 100 ns MD trajectories from each system. As depicted in Table 5, the average binding free energy values for the ER α receptor with AM and [125 I]I-AM are -149.990 kJ/mol and -165.427 kJ/mol, respectively, indicating that the [125 I]I-AM compound exhibits the strongest binding affinity with the ER α receptor.

Additionally, the MM-PBSA method can break down the total binding free energy into individual components, thereby aiding in understanding which interaction energies are significant in the binding process.¹⁷ For both complexes, the total nonpolar binding free energy represents the main driving force for the binding of AM and [125 I]I-AM compounds with the ER α receptor. This is particularly evident in the ER α -[125 I]I-AM complex system. $\Delta E_{\text{polar, total}}$ impedes binding, which is partially compensated for by the favorable electrostatic interaction energy ΔE_{ele} . Overall, these findings shed light on the intricate nature of the interaction between the ER α receptor and the compounds. The favorable interaction of [125 I]I-AM with the ER α receptor could be further evaluated as a potentially useful theranostic agent in the detection and treatment of breast cancer.

Synthesis

The synthetic pathway of iodinated AM is depicted in Scheme S1. N-Chlorosuccinimide (NCS) was used as an oxidizing agent to oxidize iodine. The oxidized iodine reacts with AM by an electrophilic substitution reaction. The structure of the resulting nonradioactive compound was confirmed by MS and NMR (Supporting Information). AM has electron-rich aromatic rings that enable it to be labeled with iodine through an electrophilic substitution reaction. Considering the structure of AM, carbons at positions 4 and 5 are the sites where iodine can be introduced (Figure 1). However, the concentration of radioiodine is so low²⁰ that only one iodine can be introduced into the AM stochastically. The synthesis steps began by first synthesizing an authentic compound in which one iodine was introduced with nonradioactive iodine. From the $^1\text{H-NMR}$, $^{13}\text{C-NMR}$, 2D-NMR, and mass spectrometry (Figures S1–S3), the position at which iodine was introduced was confirmed to be position 4. Therefore, it is considered that iodine is easier to be introduced at position 4 than position 5 due to the arrangement of the hydroxy groups.^{21,22}

[125 I]I-AM was prepared in a similar method as the nonradioactive compound. [125 I]I-AM depicted single peaks at retention time identical to that of nonradioactive compounds on HPLC (Figure 5b). The radiochemical yield and purity were $20.2 \pm 0.88\%$ ($n = 3$) and $>95\%$ after HPLC purification, respectively. [125 I]I-AM showed a single peak (Figure 5c) at the retention time identical to nonradioactive I-AM on HPLC, suggesting that radioiodine was introduced at position 4.

Table 5 The Binding Free Energy in the Arrangement Between AM and [125 I]I-AM Towards the ER α Receptor

Contribution	ER α – AM	ER α – [125 I]I-AM
Van der Waals interaction energy (ΔE_{vdw})	-231.580 ± 16.277 kJ/mol	-222.880 ± 15.179 kJ/mol
Electrostatic energy (ΔE_{ele})	-39.157 ± 25.530 kJ/mol	-7.860 ± 12.054 kJ/mol
Polar solvent effect energy (ΔE_{PB})	143.893 ± 28.274 kJ/mol	88.601 ± 17.833 kJ/mol
Nonpolar solvent effect energy (ΔE_{SA})	-23.146 ± 0.767 kJ/mol	-23.287 ± 1.077 kJ/mol
Polar binding free energy ($\Delta E_{\text{polar, total}}$)	0.000 ± 0.000 kJ/mol	0.000 ± 0.000 kJ/mol
Nonpolar binding free energy ($\Delta E_{\text{nonpolar, total}}$)	0.000 ± 0.000 kJ/mol	0.000 ± 0.000 kJ/mol
Binding free energy (ΔG)	-149.990 ± 14.602 kJ/mol	-165.427 ± 14.962 kJ/mol

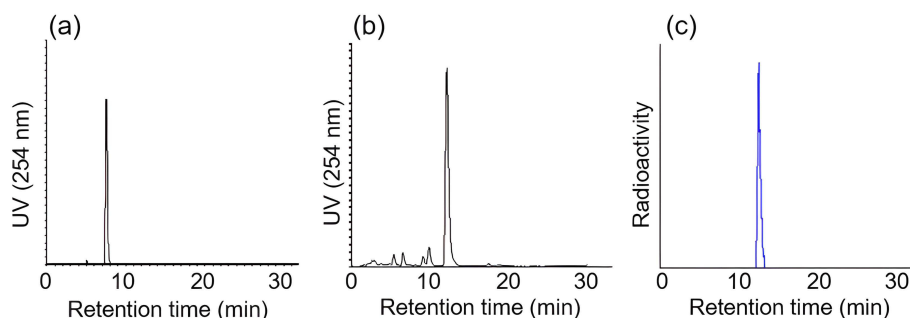


Figure 5 RP-HPLC chromatogram of (a) AM, (b) $[^{125}\text{I}]$ I-AM measured by UV detector, and (c) $[^{125}\text{I}]$ I-AM measured by radiation detector.

Log $D_{7.4}$ Determination

To estimate the lipophilicity of $[^{125}\text{I}]$ I-AM, the $\log D_{7.4}$ of $[^{125}\text{I}]$ I-AM was determined. The $\log D_{7.4}$ value of $[^{125}\text{I}]$ I-AM was 1.35 ± 0.03 indicating that $[^{125}\text{I}]$ I-AM was a lipophilic compound.

Stability in Murine Plasma

The stability of $[^{125}\text{I}]$ I-AM in murine plasma is shown in Figure 6. $[^{125}\text{I}]$ I-AM was stable after 3 hours in mice plasma with a purity of more than 95% as analyzed by HPLC.

Cellular Uptake Studies

Several studies suggested that AM would be involved in $\text{ER}\alpha$, but whether AM binds to $\text{ER}\alpha$ directly is still unclear. Therefore, the binding of $[^{125}\text{I}]$ I-AM to $\text{ER}\alpha$ was evaluated using MCF-7 breast cancer cells. The uptake of $[^{125}\text{I}]$ I-AM in the MCF7 cell line is shown in Figure 7a. The cellular uptake study was performed at 30 min, 1, and 3 h of incubation time with the percentage uptake of 13.5 ± 0.13 , 15.1 ± 0.93 , and $10.5 \pm 1.0\%$, respectively. The uptake of $[^{125}\text{I}]$ I-AM into MCF-7 cells was found to increase with time up to 1 h and then it decreases (Figure 7a). The uptake of $[^{125}\text{I}]$ I-AM was significantly inhibited by AM (Figure 7b), indicating that $[^{125}\text{I}]$ I-AM is bound to the same binding site as AM and that the introduction of iodine into AM has little effect on AM properties. Furthermore, the uptake of $[^{125}\text{I}]$ I-AM was significantly inhibited by tamoxifen, an inhibitor of $\text{ER}\alpha$. These results suggested that $[^{125}\text{I}]$ I-AM could bind to $\text{ER}\alpha$ and further suggested that AM could also bind to $\text{ER}\alpha$. To our knowledge, this is the first evidence that AM could bind to $\text{ER}\alpha$, although several studies suggested that AM would be involved in $\text{ER}\alpha$.^{16,17} On the other hand, the uptake of $[^{125}\text{I}]$ I-AM was not inhibited by estradiol, which is also an inhibitor of $\text{ER}\alpha$. It is known that both tamoxifen and estradiol could bind to $\text{ER}\alpha$, but the binding site of $\text{ER}\alpha$ is different.^{6,7} Therefore, these results suggested that $[^{125}\text{I}]$ I-AM binds to $\text{ER}\alpha$ at a site similar to the binding site of tamoxifen. This was also supported by previous docking studies.¹³ Although the data showed that $[^{125}\text{I}]$ I-AM could bind to $\text{ER}\alpha$, the binding of $[^{125}\text{I}]$ I-AM to MCF-7 cells could not be completely inhibited by tamoxifen, even at a higher concentration (1 mM). These results suggested that the selectivity of $[^{125}\text{I}]$ I-AM to $\text{ER}\alpha$ was low, although the K_d value or IC_{50} of $[^{125}\text{I}]$ I-AM to $\text{ER}\alpha$

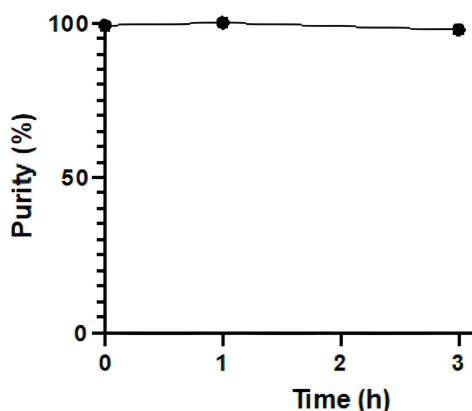


Figure 6 Percent radioactivity as intact compound after incubation of $[^{125}\text{I}]$ I-AM in murine plasma.

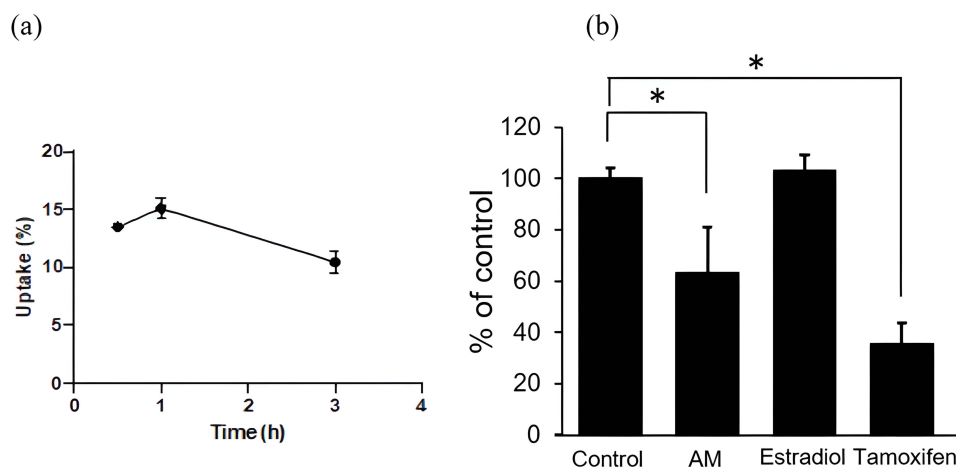


Figure 7 (a) The uptake of $[^{125}\text{I}]\text{-AM}$ in MCF-7 cells from 0.5 h to 3 h was determined (b) The uptake of $[^{125}\text{I}]\text{-AM}$ was measured in the presence or absence of AM (1 mM), estradiol (1 mM), and tamoxifen (1 mM). * $p < 0.05$.

was not determined in this study. However, these results were not surprising as AM has demonstrated various pharmacological effects including anti-cancer, anti-inflammatory, antioxidant, antiviral, antibacterial, and anti-allergic activities,^{23–26} which means that it also has the potential to bind with other receptors.

Furthermore, this study also shows the ability of $[^{125}\text{I}]\text{-AM}$ to bind on $\text{ER}\alpha$, although the binding was unspecific. Clinically, several radiopharmaceuticals targeting the $\text{ER}\alpha$ in breast cancer have been developed and this includes F-18 labeled estradiol derivatives.²⁷ Based on these considerations, the applicability of radioiodinated-AM as a breast cancer imaging agent was determined using ^{125}I radioiodine. ^{125}I was chosen due to its long half-life, commercially available, and easy to use in the laboratory. In addition, ^{125}I can be replaced by other radioiodines for therapeutic (^{131}I) and diagnostic ($^{123/131}\text{I}$) purposes without affecting its chemical and biological properties.²⁸

Biodistribution Studies

The finding from the biodistribution study of $[^{125}\text{I}]\text{-AM}$ in normal mice is illustrated in Tables 6 and 7. Ten min after injection, the accumulation of $[^{125}\text{I}]\text{-AM}$ was observed in the liver, stomach, intestine, and kidney. Thereafter, the radioactivity in the liver and kidney decreases with time. On the other hand, radioactivity in the stomach, intestine, and neck remained high. The $\text{LogD}_{7.4}$ of $[^{125}\text{I}]\text{-AM}$ was 1.35, indicating $[^{125}\text{I}]\text{-AM}$ was highly lipophilic. Therefore, $[^{125}\text{I}]\text{-AM}$

Table 6 Biodistribution of Radioactivity After Intravenous Injection of $[^{125}\text{I}]\text{-AM}$ in Normal Mice

	Time after Injection				
	10 min	1 h	3 h	6 h	24 h
Blood ^b	3.83 ± 0.49	2.16 ± 0.40	1.29 ± 0.20	0.52 ± 0.16	0.06 ± 0.01
Liver ^b	8.55 ± 1.19	1.52 ± 0.28	1.17 ± 0.14	0.54 ± 0.11	0.14 ± 0.01
Spleen ^b	2.01 ± 0.09	1.40 ± 0.22	0.91 ± 0.22	0.37 ± 0.15	0.04 ± 0.01
Kidney ^b	5.41 ± 0.55	3.95 ± 0.93	2.14 ± 1.03	0.63 ± 0.16	0.08 ± 0.01
Pancreas ^b	2.02 ± 0.26	1.29 ± 0.43	0.80 ± 0.17	0.30 ± 0.07	0.03 ± 0.02
Heart ^b	1.87 ± 0.18	0.87 ± 0.20	0.59 ± 0.13	0.25 ± 0.07	0.13 ± 0.22
Lung ^b	3.07 ± 0.48	2.04 ± 0.46	1.16 ± 0.27	0.45 ± 0.08	0.38 ± 0.71
Stomach ^{a*}	7.61 ± 0.78	15.0 ± 5.62	10.3 ± 2.55	5.90 ± 2.08	0.25 ± 0.24
Intestine ^a	6.70 ± 1.33	6.28 ± 1.70	10.0 ± 1.43	4.56 ± 1.96	0.08 ± 0.07
Muscle ^b	1.00 ± 0.13	0.60 ± 0.07	0.51 ± 0.43	0.15 ± 0.03	0.02 ± 0.01
Bone ^b	1.52 ± 0.25	0.86 ± 0.11	0.70 ± 0.12	0.36 ± 0.09	0.02 ± 0.02
Neck ^{a*}	0.58 ± 0.14	3.25 ± 0.80	5.05 ± 1.52	6.65 ± 0.62	5.29 ± 1.41

Notes: ^a Expressed as %ID/g, ^b Expressed as %ID. Mean ± S.D. of four to five animals for each point, * high radioactivity levels.

Table 7 Biodistribution of Radioactivity After Intravenous Injection of [¹²⁵I]I-AM in Tumor-Bearing Mice

	Time after Injection	
	1 h	3 h
Blood ^b	3.22 ± 0.71	1.93 ± 0.90
Liver ^b	3.47 ± 2.30	2.26 ± 1.53
Spleen ^b	2.21 ± 0.89	1.26 ± 0.56
Kidney ^b	4.05 ± 1.85	1.82 ± 0.79
Pancreas ^b	2.33 ± 1.01	0.98 ± 0.30
Heart ^b	1.23 ± 0.24	0.80 ± 0.24
Lung ^b	2.99 ± 0.77	1.68 ± 0.72
Stomach ^{a*}	8.38 ± 1.66	3.99 ± 2.34
Intestine ^a	13.9 ± 10.11	15.1 ± 8.28
Muscle ^b	0.85 ± 0.31	0.86 ± 0.65
Bone ^b	1.39 ± 0.33	0.79 ± 0.33
Neck ^{a*}	2.11 ± 0.47	6.04 ± 2.83
Tumor ^b	2.03 ± 1.35	1.16 ± 0.42
Tumor/Blood ^b	0.60 ± 0.30	0.63 ± 0.15
Tumor/Muscle ^b	2.41 ± 0.97	1.72 ± 0.98

Notes: ^a Expressed as %ID/g, ^b Expressed as %ID, Mean ± S.D. of four to five animals for each point, * high radioactivity levels.

I-AM would be accumulated in the liver and excreted into the intestine via the bile, as in the case of FES.²⁹ On the other hand, high radioactivity levels were observed in the stomach and neck (containing thyroid) from 10 min to 24 h post-injection of [¹²⁵I]I-AM. Because free iodine (I⁻) was accumulated in these tissues,^{29,30} the results suggested that [¹²⁵I]I-AM was unstable against *in vivo* deiodination. In an *in vitro* study, a decrease in radioactivity in MCF-7 cells at 3 h was observed (Figure 4a). This result suggested that [¹²⁵I]I-AM was deiodinated after internalizing into the cells.

In this study, the introduction of iodine into AM was at the ortho position of the phenolic hydroxy group. In general, the introduction of iodine at the ortho position of the phenolic hydroxy group was readily deiodinated *in vivo*, as shown by radioiodinated L-tyrosine and Bolton-Hunter reagent.³¹ Therefore, the deiodination of [¹²⁵I]I-AM would have occurred in the body. Similar results have been reported for natural products labeled with radioiodine, such as ¹³¹I-labeled hydroxytyrosol,³² ¹²³I-labeled hesperetin,³³ ¹²⁵I-labeled rutin,³⁴ and ¹²⁵I-labeled khellin.³⁵ Because the structures of natural products are complex, it is rather challenging to modify the structure while preserving the original properties. Therefore, the low stability against deiodination becomes a big challenge in the radiolabeling process of natural products.³⁶

Experimental Section

Computational Methodology

Calculated Structure of [¹²⁵I]I-AM Complex

The compounds employed as a model in this investigation were AM and [¹²⁵I]I-AM. Each molecule underwent optimization utilizing Gaussian 09 and GausView 05 software.³⁵ Density Functional Theory (DFT) methodology was employed for the calculations, employing the Becke, 3-parameter, Lee–Yang–Parr (B3LYP) level and a 6–31G basis set for the free-base AM, while the LANL2DZ basis set was utilized for the [¹²⁵I]I-AM complexes.³⁵ After the optimization of the molecules, structural parameter calculations were conducted to forecast the stability of the [¹²⁵I]I-AM complexes. The determination of HOMO and LUMO energies ensued to ascertain the DFT global chemical reactivity descriptor.

The DFT global chemical reactivity descriptors, which encompass the chemical potential (μ), global hardness (η), and electrophilicity (ω), are determined through the following formulas:

$$\eta = (I - A)/2 \quad (1)$$

$$\mu = (I + A)/2 \quad (2)$$

$$\omega = \mu^2/2\eta \quad (3)$$

In these equations, (I) represents the ionization energy, while (A) stands for the electron affinity of the electron system (neutral or charged) under examination. These parameters are derived using the orbital theory method by assessing the LUMO and HOMO energies to determine the ionization energy and electron affinity, respectively.

Molecular Docking Studies [¹²⁵I]I-AM Against ER α

Molecular docking was conducted using the AutoDock software in conjunction with the Perl script.³⁵ The preparation of the ER α receptor structure involved cleaning it from water and adhering ligands using AutoDock Tools 4.2.6. The ER α receptor structure utilized in this study was sourced from the Protein Data Bank under PDB ID: 3ERT (<https://www.rcsb.org/structure/3ERT>).³⁷ This structure represents the receptor in a complex with tamoxifen, which serves as the native ligand. Subsequently, hydrogen atoms were eliminated, polar hydrogens were reintroduced, and Kolmann charges were appended. A grid box was then positioned over the active site of the ER α receptor enzyme encompassing amino acids surrounding the binding site, representing the catalytic site. The coordinates and dimensions of the grid box were recorded for future use in the input file, while the prepared protein structure was saved in the PDBQT format. Creation of the configuration file followed, detailing receptor and ligand file names, grid box size and position, the number of molecular docking iterations, the number of computational threads utilized, and log file names.

The molecular docking outcomes included information on the ligand's binding affinity and its conformation when bound to the ER α receptor. Evaluation of the molecular docking results was performed using AutoDock, focusing on binding affinity and intermolecular interaction locations. Ligands with accurate positioning were retained and visually inspected for intermolecular interactions via Discovery Studio software. Visualization using Discovery Studio allowed the examination of intermolecular interactions in two dimensions (2D).³⁵ The most favorable conformation with the lowest energy value was stored in PDB format for subsequent molecular dynamics simulations.

Molecular Dynamics Simulations [¹²⁵I]I-AM Against ER α

To verify the accuracy of the docking outcomes, a molecular dynamics simulation (MD) of the complexes was executed. Using the GROMACS-2016.3 software package, MD simulations lasting 100 ns were conducted on the best docking configurations of ER α -AM and ER α -[¹²⁵I]I-AM complexes from the molecular docking study.³⁵ The AMBER99SB force field was employed for the simulations. The force field parameters for the ligands were generated using the AnteChamber PYthon Parser interface (ACPYPE).³⁵ The complexes were solvated using the TIP3P water model, and sodium and chloride ions were added for neutralization. Periodic boundary conditions (PBC) were applied, and energy minimization was performed with a force tolerance of 1000 kJ/mol/nm. Subsequently, the system was equilibrated in the NVT and NPT ensembles for 1 ns. To ensure overall charge neutrality and an ionic strength of 0.15 M, sodium and chloride counter-ions were added as needed. An energy minimization procedure was employed initially to alleviate significant forces and relax the simulated systems, followed by a relaxation process. Temperature and pressure were maintained at 310 K and 1.0 bar, respectively, using the Nose-Hoover thermostat and the Berendsen barostat. Trajectories were saved every 2 ps, with data points generated every 2 fs. Post-MD analyses included root mean square deviation (RMSD), root mean square fluctuations (RMSF), the radius of gyration (Rg), solvent-accessible surface area (SASA), secondary structure, and hydrogen bond occupancy.

Binding Free Energy Calculations [¹²⁵I]I-AM Against ER α

The stable MD trajectory obtained from each system was selected to compute the average binding free energies (ΔG) using the MM-PBSA approach from the GROMACS-2016.3 program.³⁵ A total of 100 snapshots were extracted from the 100 ns MD trajectories at 100 ps intervals. In essence, the MM-PBSA method involves several steps:

$$\Delta G = G_{\text{complex}} - (G_{\text{protein}} + G_{\text{ligand}}) \quad (4)$$

$$G = E_{MM} + G_{\text{sol}} - T\Delta S \quad (5)$$

$$E_{MM} = E_{\text{vdw}} + E_{\text{ele}} \quad (6)$$

$$G_{\text{sol}} = E_{PB} + E_{SA} \quad (7)$$

$$E_{SA} = \gamma \times SASA \quad (8)$$

$$\Delta G = \Delta E_{\text{vdw}} + \Delta E_{\text{ele}} + \Delta E_{PB} + \Delta E_{SA} \quad (9)$$

The free energy of the complex (G_{complex}), protein (G_{protein}), and ligand (G_{ligand}) are calculated (Equation 4). The overall free energy (G) (Equation 5) comprises the gas-phase binding energy (E_{MM}), solvation-free energy (G_{sol}), and entropic contribution ($T\Delta S$). E_{MM} consists of van der Waals (E_{vdw}) and electrostatic (E_{ele}) terms (Equation 6), while G_{sol} includes polar (E_{PB}) and nonpolar (E_{SA}) components (Equation 7). The polar solvation term is determined using the Poisson–Boltzmann model, and the nonpolar term is based on solvent-accessible surface area (SASA) calculations with a default value for γ (Equation 8).

However, accounting for entropy ($T\Delta S$) is computationally demanding, and its inclusion in ΔG does not always guarantee the accuracy of binding free energy calculations. Hence, in this study, only the relative binding free energy without the entropic effect was calculated to determine the binding affinity between the ER α receptor and the AM and [^{125}I]I-AM compounds (Equation 9). Free energy decomposition to individual residues was also performed to identify the key residues responsible for binding, using the same snapshots utilized in the aforementioned calculations.

Chemistry

[^{125}I]NaI was purchased from Perkin Elmer Japan (Yokohama, Japan). AM was purchased from Biopurify (Chengdu, China). Tamoxifen was purchased from Combi Blocks (CA, USA). Other chemicals purchased from commercial sources were of reagent grade or higher and used without further purification. Flash column chromatography (Biotage Japan, Tokyo, Japan) was performed using a prepacked silica gel column (Purif-Pack[®]-EX-SI-50 μm , Shoko Science Co. Ltd., Yokohama). ^1H NMR/ ^{13}C NMR spectra were recorded using a JEOL ECS-400 spectrometer (JEOL, Tokyo) and heteronuclear multiple bond coherence (HMBC) spectra were measured using JEOL ECS-600 spectrometer using residual solvents as the internal standard. The coupling constants were expressed in hertz. Mass spectrometry was obtained on an AccuTOF LC-plus (JMS-T100LP, JEOL). Reversed-phase HPLC (RP-HPLC) purification and analysis were conducted with RP-C18 column (250 \times 4.6 mm, Unison US-C18, Imtakt, Kyoto, Japan) at a flow rate of 1 mL/min with a mobile phase maintained 20% A (0.1% aqueous trifluoro acetic acid (TFA)) and 80% B (0.1% TFA in acetonitrile) for 20 min, then gradually changed to 0% A and 100% B at 30 min.

Synthesis of Nonradioactive Compound

AM (50 mg, 0.12 mmol) and N-Chlorosuccinimide (NCS, 16.3 mg, 0.12 mmol) were dissolved in the mixture of methanol: acetic acid (100: 1 (v/v), 2 mL). Then, sodium iodide (18.3 mg, 0.12 mmol) was added to the mixture and stirred at room temperature for 2 h. After the solution was concentrated under reduced pressure, the reaction mixture was purified by flash column chromatography using hexane: ethyl acetate (77: 33) to afford yellow solid (10.5 mg, 20.9%). The objective compound was identified by mass spectrometry and NMR spectra. ^1H -NMR (CDCl_3) δ : 1.69 [3H, s, CH_3], 1.73 [3H, s, CH_3], 1.83 [6H, s, CH_3], 3.49 [2H, d, CH_2 , $J=6.86$ hz], 3.81 [3H, s, OCH_3], 4.08 [2H, d, CH , $J=5.49$ hz], 5.18–5.31 [2H, m, CH], 6.36 [2H, br, OH], 6.98 [1H, s, CH], 13.78 [1H, s, OH]; ^{13}C -NMR (CDCl_3) δ : 17.9, 18.2, 22.6, 25.8, 25.9, 26.5, 61.3, 62.1, 101.9, 104.5, 110.0, 111.7, 121.3, 122.9, 132.3, 134.1, 137.1, 143.0, 153.2, 154.9, 155.6, 159.4, 161.2, 181.7; ESI-MS m/z [$\text{M} + \text{H}$]⁺ 535, Found 535 as shown in [Figure S4](#).

Preparation of Radioactive Compound

AM (50 µg, 0.12 µmol) was dissolved in the mixture of methanol: acetic acid (100: 1 (v/v), 50 µL) and then [¹²⁵I]NaI (0.37–3.7 MBq, 1.0 µL) was added to the solution. NCS (1 µg/µL, 50 µL) was then added to the solution and incubated for 15 min at room temperature. The reaction was stopped by the addition of Na₂S₂O₅ (1 µg/µL, 7 µL). The reaction mixture was subjected to RP-HPLC to obtain [¹²⁵I]I-AM. The collected fraction was neutralized with a 1 N NaOH, and the solvent was concentrated under reduced pressure.

Partition Coefficient

n-Octanol (1 mL) and 0.1 M phosphate buffer saline (PBS) (0.8 mL, pH 7.4) were mixed and equilibrated for 24 h. [¹²⁵I]I-AM (370 kBq, 0.2 mL) was dissolved in PBS and added to the equilibrated mixture. The mixture was vigorously shaken for 1 min and left to stand for 1 min. This shaking cycle was repeated three times, and the mixture was left to stand for 20 min. Next, the mixture was fractionated into an organic layer and an aqueous layer by centrifugation (4 °C, 1500 g × 5 min). The radioactivity in each layer was measured with a gamma counter. Each experiment was conducted three times. The logD_{7.4} values were calculated using the following equation:

$$\log D_{7.4} = \log (\text{radioactivity of organic layer} / \text{radioactivity of aqueous layer}).$$

In Vitro Stability Estimation

In vitro stability was performed on PBS and freshly prepared murine plasma. [¹²⁵I]I-AM (37 KBq, 50 µL PBS) was added to 450 µL of PBS or murine plasma and then incubated at 37 °C for 1 and 3 h. Aliquots (200 µL) were withdrawn at 1 and 3 h into microcentrifuge tubes and mixed with an equal volume of ethanol to precipitate plasma proteins, followed by centrifugation (4 °C, 1700 g × 5 min). Then, the supernatant was filtrated (0.45 µm) and analyzed by RP-HPLC.

Cellular Uptake Assay

MCF-7 cells that purchased from ATCC (Manassas, VA) or supplied from Cell Resource Center for Biomedical Research, Institute of Development, Aging and Cancer Tohoku University were grown in MEM medium supplemented with 10% (v/v) fetal bovine serum, streptomycin (100 µg/mL), and penicillin (100 U/mL) in a humidified atmosphere containing 5% CO₂ at 37 °C. The MCF-7 cells were seeded at a density of 3 × 10⁵ cells/well (0.5 mL) in 24-well plates and incubated for 24 h. The culture medium was removed, and cells were washed 2 times with PBS (0.5 mL). The FBS(-) MEM medium with 0.2% BSA (450 µL) and [¹²⁵I]I-AM (370 kBq with 1%DMSO, 50 µL) was added into the wells, and incubated for 30 min, 1 h, and 3 h in a humidified atmosphere containing 5% CO₂ at 37 °C. After removing the medium, cells were washed with ice-cold PBS (0.5 mL) and dissolved in 0.1 N NaOH (0.5 mL). The radioactivity of the medium phase and cell lysate (NaOH phase) was measured by a gamma counter. Cellular uptake was calculated as a percentage of the radioactivity in cell lysate per total radioactivity. To determine the uptake pathway of [¹²⁵I]I-AM into the cells, the MCF-7 cells were treated separately with AM, tamoxifen, and 17 β -estradiol, all at a concentration of 1 mM.

Biodistribution Studies

Animal studies were conducted in accordance with the guidelines of Chiba University after being approved by the Chiba University Animal Care Committee (Approval No. Dou4-387). [¹²⁵I]I-AM (100 µL (1% DMSO in PBS), 7.4 kBq/mouse) was intravenously injected to 5-week-old male ddY mice (n = 5). At 10 min, 1 h, 3 h, 6 h, and 24 h post-injection, the mice were sacrificed, and blood and the organs of interest were dissected. Each tissue of interest was excised and weighed, and the radioactivity counts were determined with a gamma counter. Urine and feces were collected for 24 h following the injection of [¹²⁵I]I-AM, and their radioactivity was also measured. The data were expressed as the percent injected dose (%ID) for the stomach, intestine, and thyroid gland, or the percent injected dose per gram of tissue (%ID/g) for other organs.

The tumor-bearing mice were prepared by the subcutaneous injection of MCF-7 cells (5 × 10⁶ cells suspended in 100 µL of PBS: Matrigel = 1:1 (v/v)) into the right flank of 5-week-old female BALB/c *nu/nu* mice (Japan SLC, Inc).

When the tumor size reached 0.5–1.0 cm in diameter, the mice were used for biodistribution study. [¹²⁵I]I-AM (100 μL (1% DMSO in PBS), 7.4 kBq/mouse) was intravenously injected into the model mice (n = 5). At 1 h and 3 h post-injection, the mice were sacrificed and dissected. The evaluation was performed in the same manner as described above.

Statistical Analysis

Cellular uptake with a blocking agent was analyzed using *one-way* ANOVA followed by Tukey's multiple comparison test (GraphPad Prism, CA). Significance was assigned at $p < 0.05$.

Conclusion

In conclusion, the results of the molecular docking and MM-PBSA analyses indicate that [¹²⁵I]I-AM demonstrates superior binding affinity to the ER α receptor compared to AM, with energy values of -9.09 kcal/mol and -7.99 kcal/mol for molecular docking, and -165.427 kJ/mol versus -149.990 kJ/mol for MM-PBSA, respectively. These findings suggest that the cellular uptake of [¹²⁵I]I-AM is partly mediated by ER α and that it shows significant tumor accumulation in vivo, although the deiodination of the compound occurs. To enhance its effectiveness and stability, further research is needed to address the issue of deiodination. Overall, [¹²⁵I]I-AM represents a promising platform for developing new radiopharmaceuticals targeting ER α , potentially advancing theranostic applications for breast cancer treatment. Continued optimization and evaluation could lead to improved personalized treatment strategies and more effective targeted imaging and therapy.

Abbreviation

%ID, Percentage of the injected dose of organs; %ID/gram, Percentage of injected dose per dram organs; 4-OHT, 4-Hydroxytamoxifen; AM, Alpha-mangostin; BSA, Bovine serum albumin; ER, Estrogen receptor; FBS, Fetal bovine serum; HPLC, High performance chromatography; MCF7, Michigan Cancer Foundation-7; MEM, Minimum essential medium; MS, Mass spectrometry; NMR, Nuclear magnetic resonance; PBS, Phosphate buffer saline; DFT, Density Functional Theory; HOMO, Highest Occupied Molecular Orbital; LUMO, Lowest Unoccupied Molecular Orbital; RMSD, Root mean square deviation; RMSF, Root mean square fluctuation; Rg, Radius of gyration; SASA, Solvent-accessible surface area.

Institutional Review Board Statement

Animal studies were conducted in accordance with the institutional guidelines approved by the Chiba University Animal Care Committee (No. 4-182, 4-185, 4-387).

Acknowledgments

The authors thank Ministry of Education Culture, Research, and Technology, Directorate General of Higher Education, Research, and Technology Republic of Indonesia, for supporting this study through PMDSU scholarship and the PKPI-PMDSU program.

Author Contributions

All authors made a significant contribution to the work reported, whether that is in the conception, study design, execution, acquisition of data, analysis and interpretation, or in all these areas; took part in drafting, revising or critically reviewing the article; gave final approval of the version to be published; have agreed on the journal to which the article has been submitted; and agree to be accountable for all aspects of the work.

Funding

This research was funded by Applied Research and PMDSU Grants of the Ministry of Education Culture, Research, and Technology, grant number 044/E5/PG.02.00.PL/2023. This study was supported by a management expense grant from Chiba University.

Disclosure

The authors report no conflicts of interest in this work.

References

1. Bray F, Laversanne M, Sung H, et al. Global cancer statistics 2022: GLOBOCAN estimates of incidence and mortality worldwide for 36 cancers in 185 countries. *CA Cancer J Clin.* 2024;74:229–263. doi:10.3322/caac.21834
2. Coughlin SS, Ekwueme DU. Breast cancer as a global health concern. *Cancer Epid.* 2009;33:315–318. doi:10.1016/j.canep.2009.10.003
3. Ferlay J, Colombet M, Soerjomataram I, et al. Cancer statistics for the year 2020: an overview. *Inter J Cancer.* 2021;149:778–789. doi:10.1002/ijc.33588
4. Arnold M, Morgan E, Rumgay H, et al. Current and future burden of breast cancer: global statistics for 2020 and 2040. *Breast.* 2022;66:15–23. doi:10.1016/j.breast.2022.08.010
5. Lippman ME, Allegra JC. Current concepts in cancer. Receptors in breast cancer. *N Engl J Med.* 1978;299:930–933. doi:10.1056/nejm197810262991706
6. Lonard DM, Smith CL. Molecular perspectives on selective estrogen receptor modulators (SERMs): progress in understanding their tissue-specific agonist and antagonist actions. *Steroids.* 2002;67:15–24. doi:10.1016/s0039-128x(01)00133-7
7. Jameera Begam A, Jubie S, Nanjan MJ. Estrogen receptor agonists/antagonists in breast cancer therapy: a critical review. *Bioorg Chem.* 2017;71:257–274. doi:10.1016/j.bioorg.2017.02.011
8. Anbalagan M, Rowan BG. Estrogen receptor alpha phosphorylation and its functional impact in human breast cancer. *Mole Cell Endocrinol.* 2015;418:264–272. doi:10.1016/j.mce.2015.01.016
9. Li P, Tian W, Ma X. Alpha-mangostin inhibits intracellular fatty acid synthase and induces apoptosis in breast cancer cells. *Mol Cancer.* 2014;13:138. doi:10.1186/1476-4598-13-138
10. Ibrahim M, Mohd Hashim N, Mohan S, et al. α -Mangostin from *Cratoxylum arborescens* demonstrates apoptosis in MCF-7 with regulation of NF- κ B and Hsp70 protein modulation in vitro, and tumor reduction in vivo. *Drug Des Dev Ther.* 2014;2014:1629–1647. doi:10.2147/DDDT.S66105
11. Shibata M-A, Iinuma M, Morimoto J, et al. α -Mangostin extracted from the pericarp of the mangosteen (*Garcinia mangostana*Linn) reduces tumor growth and lymph node metastasis in an immunocompetent xenograft model of metastatic mammary cancer carrying a p53 mutation. *BMC Med.* 2011;9:69. doi:10.1186/1741-7015-9-69
12. Gunter NV, Teh SS, Jantan I, Cespedes-Acuña CL, Mah SH. The mechanisms of action of prenylated xanthenes against breast, colon, and lung cancers, and their potential application against drug resistance. *Phytochem Rev.* 2022. doi:10.1007/s11101-022-09846-9
13. Muchtaridi M, Dermawan D, Yusuf M. Molecular docking, 3D structure-based pharmacophore modeling, and ADME prediction of alpha mangostin and its derivatives against estrogen receptor alpha. *J Young Pharma.* 2018;10:252. doi:10.5530/jyp.2018.10.58
14. Mardianingrum R, Yusuf M, Hariyono M, Mohd Gazzali A, Muchtaridi M. α -Mangostin and its derivatives against estrogen receptor alpha. *J Biomol Struc Dyn.* 2022;40:2621–2634. doi:10.1080/07391102.2020.1841031
15. Muchtaridi M, Megantara S, Dermawan D, Yusuf M. Antagonistic mechanism of α -mangostin derivatives against human estrogen receptor α of breast cancer using molecular dynamics simulation. *Rasayan J Chem.* 2019;12:1927–1934. doi:10.31788/RJC.2019.1245391
16. Setiawati A, Octa F, Riswanto D, Yuliani SH, Istyastono E. Anticancer activity of mangosteen pericarp dry extract against MCF-7 breast cancer cell line through estrogen receptor alpha. *Indo J Pharm.* 2014;25:119–124. doi:10.14499/indonesianjpharm25iss3pp119
17. Won Y-S, Lee J-H, Kwon S-J, et al. α -Mangostin-induced apoptosis is mediated by estrogen receptor α in human breast cancer cells. *Food Chem Tox.* 2014;66:158–165. doi:10.1016/j.fct.2014.01.040
18. Heldring N, Pike A, Andersson S, et al. Estrogen receptors: how do they signal and what are their targets. *Physiol Rev.* 2007;87:905–931. doi:10.1152/physrev.00026.2006
19. Huang P, Chandra V, Rastinejad F. Structural overview of the nuclear receptor superfamily: insights into physiology and therapeutics. *Annu Rev Physiol.* 2010;72:247–272. doi:10.1146/annurev-physiol-021909-135917
20. Vaidyanathan G, Zalutsky M. The radiopharmaceutical chemistry of the radioisotopes of iodine. In: *Radiopharmaceutical Chemistry*. Springer; 2019:391–408. doi:10.1007/978-3-319-98947-1_22
21. Dubost E, McErlain H, Babin V, Sutherland A, Cailly T. Recent advances in synthetic methods for radioiodination. *J Org Chem.* 2020;85:8300–8310. doi:10.1021/acs.joc.0c00644
22. Yamamoto T, Toyota K, Morita N. An efficient and regioselective iodination of electron-rich aromatic compounds using N-chlorosuccinimide and sodium iodide. *Tetra Lett.* 2010;51:1364–1366. doi:10.1016/j.tetlet.2009.12.125
23. Chae H-S, Oh S-R, Lee H-K, Joo SH, Chin Y-W. Mangosteen xanthenes, α - and γ -mangostins, inhibit allergic mediators in bone marrow-derived mast cell. *Food Chem.* 2012;134:397–400. doi:10.1016/j.foodchem.2012.02.075
24. Gan C-Y, Latiff AA. Extraction of antioxidant pectic-polysaccharide from mangosteen (*Garcinia mangostana*) rind: optimization using response surface methodology. *Carbo Poly.* 2011;83:600–607. doi:10.1016/j.carbpol.2010.08.025
25. Kosem N, Ichikawa K, Utsumi H, Moongkarndi P. In vivo toxicity and antitumor activity of mangosteen extract. *J Nat Med.* 2013;67:255–263. doi:10.1007/s11418-012-0673-8
26. Pothitirat W, Chomnawang MT, Gritsanapan W. Anti-acne-inducing bacterial activity of mangosteen fruit rind extracts. *Med Princ Pract.* 2010;19:281–286. doi:10.1159/000312714
27. Huang H, Li K, Lv G, et al. One-step (18)F-labeling of estradiol derivative for PET imaging of breast cancer. *Contrast Med Mol Imag.* 2018;2018:5362329. doi:10.1155/2018/5362329
28. El-Kawy OA, Abdelaziz G. Preparation, characterization and evaluation of [125I]-pirarubicin: a new therapeutic agent for urinary bladder cancer with potential for use as theranostic agent. *Appl Rad Isotop.* 2022;179:110007. doi:10.1016/j.apradiso.2021.110007
29. Spetz J, Rudqvist N, Forssell-Aronsson E. Biodistribution and dosimetry of free 211At, 125I- and 131I- in rats. *Cancer Biotherm Radiopharm.* 2013;28:657–664. doi:10.1089/cbr.2013.1483

30. Vallabhajosula S, Killeen RP, Osborne JR. Altered biodistribution of radiopharmaceuticals: role of radiochemical/pharmaceutical purity, physiological, and pharmacologic factors. *Semin Nucl Med.* 2010;40:220–241. doi:10.1053/j.semnuclmed.2010.02.004
31. Cavina L, van der Born D, Klaren PHM, Feiters MC, Boerman OC, Rutjes F. Design of radioiodinated pharmaceuticals: structural features affecting metabolic stability towards in vivo deiodination. *European J Org Chem.* 2017;2017:3387–3414. doi:10.1002/ejoc.201601638
32. Ozkan M, Muftuler F, Yurt A, Medine I, Unak P. Isolation of hydroxytyrosol from olive leaves extract, radioiodination and investigation of bioaffinity using in vivo/in vitro methods. *Radiochim Acta.* 2013;101:585–593. doi:10.1524/ract.2013.2068
33. Jeon J, Ma S-Y, Choi D, et al. Radiosynthesis of ¹²³I-labeled hesperetin for biodistribution study of orally administered hesperetin. *J Radioanal Nucl Chem.* 2015;306:437–443. doi:10.1007/s10967-015-4093-6.
34. Choi MH, Rho JK, Kang JA, et al. Efficient radiolabeling of rutin with ¹²⁵I and biodistribution study of radiolabeled rutin. *J Radioanal Nucl Chem.* 2016;308:477–483. doi:10.1007/s10967-015-4415-8
35. Khater SI, Kandil SA, Hussien H. Preparation of radioiodinated khellin for the urinary tract imaging. *J Radioanal Nucl Chem.* 2013;295:1939–1944. doi:10.1007/s10967-012-2250-8
36. Nurhidayah W, Setyawati LU, Daruwati I, Gazzali AM, Subroto T, Muchtaridi M. Future prospective of radiopharmaceuticals from natural compounds using iodine radioisotopes as theranostic agents. *Molecules.* 2022;27:8009. doi:10.3390/molecules27228009.
37. Shiau AK, Barstad D, Loria PM, et al. The structural basis of estrogen receptor/coactivator recognition and the antagonism of this interaction by tamoxifen. *Cell.* 1998;95:927–937. doi:10.1016/s0092-8674(00)81717-1

Drug Design, Development and Therapy

Dovepress

Publish your work in this journal

Drug Design, Development and Therapy is an international, peer-reviewed open-access journal that spans the spectrum of drug design and development through to clinical applications. Clinical outcomes, patient safety, and programs for the development and effective, safe, and sustained use of medicines are a feature of the journal, which has also been accepted for indexing on PubMed Central. The manuscript management system is completely online and includes a very quick and fair peer-review system, which is all easy to use. Visit <http://www.dovepress.com/testimonials.php> to read real quotes from published authors.

Submit your manuscript here: <https://www.dovepress.com/drug-design-development-and-therapy-journal>